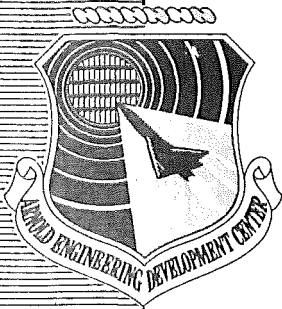


cy.1

ARCHIVE COPY
DO NOT LOAN



AEROTHERMAL TESTS OF THE SPACE SHUTTLE EXTERNAL TANK INSULATING MATERIAL

VON KÁRMÁN GAS DYNAMICS FACILITY
ARNOLD ENGINEERING DEVELOPMENT CENTER
AIR FORCE SYSTEMS COMMAND
ARNOLD AIR FORCE STATION, TENNESSEE 37389

November 1975

Final Report for Period January 12 — February 13, 1975

Approved for public release; distribution unlimited.

AEDC TECHNICAL LIBRARY



Prepared for

NATIONAL AERONAUTICS AND SPACE ADMINISTRATION (MSFC)
MARSHALL SPACE FLIGHT CENTER, ALABAMA 35812

Property of U.S. Air Force
AEDC LIBRARY
F40600-75-C-0001

NOTICES

When U. S. Government drawings specifications, or other data are used for any purpose other than a definitely related Government procurement operation, the Government thereby incurs no responsibility nor any obligation whatsoever, and the fact that the Government may have formulated, furnished, or in any way supplied the said drawings, specifications, or other data, is not to be regarded by implication or otherwise, or in any manner licensing the holder or any other person or corporation, or conveying any rights or permission to manufacture, use, or sell any patented invention that may in any way be related thereto.

Qualified users may obtain copies of this report from the Defense Documentation Center.

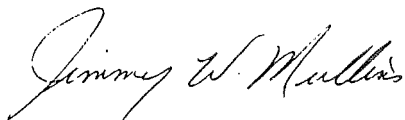
References to named commercial products in this report are not to be considered in any sense as an endorsement of the product by the United States Air Force or the Government.

This report has been reviewed by the Information Office (OI) and is releasable to the National Technical Information Service (NTIS). At NTIS, it will be available to the general public, including foreign nations.

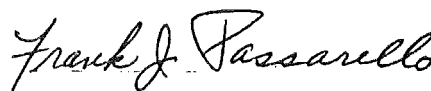
APPROVAL STATEMENT

This technical report has been reviewed and is approved for publication.

FOR THE COMMANDER



JIMMY W. MULLINS
Lt Colonel, USAF
Chief Air Force Test Director, VKF
Directorate of Test



FRANK J. PASSARELLO
Colonel, USAF
Director of Test

UNCLASSIFIED

| REPORT DOCUMENTATION PAGE | | READ INSTRUCTIONS BEFORE COMPLETING FORM |
|--|-----------------------|---|
| 1. REPORT NUMBER AEDC-TR-75-94 | 2. GOVT ACCESSION NO. | 3. RECIPIENT'S CATALOG NUMBER |
| 4. TITLE (and Subtitle) AEROTHERMAL TESTS OF THE SPACE SHUTTLE EXTERNAL TANK INSULATING MATERIAL | | 5. TYPE OF REPORT & PERIOD COVERED Final Report, Jan 12 - Feb 13, 1975 |
| | | 6. PERFORMING ORG. REPORT NUMBER |
| 7. AUTHOR(s) R. K. Matthews, ARO, Inc., and D. C. Harper, Captain, USAF | | 8. CONTRACT OR GRANT NUMBER(s) |
| 9. PERFORMING ORGANIZATION NAME AND ADDRESS Arnold Engineering Development Center (XO) Arnold Air Force Station, TN 37389 | | 10. PROGRAM ELEMENT, PROJECT, TASK AREA & WORK UNIT NUMBERS Program Element 921E |
| 11. CONTROLLING OFFICE NAME AND ADDRESS National Aeronautics and Space Admin- istration (NASA/MSFC/EE31), Marshall Space Flight Center, Alabama 35812 | | 12. REPORT DATE November 1975 |
| 14. MONITORING AGENCY NAME & ADDRESS (if different from Controlling Office) | | 13. NUMBER OF PAGES 36 |
| | | 15. SECURITY CLASS. (of this report) UNCLASSIFIED |
| | | 15a. DECLASSIFICATION/DOWNGRADING SCHEDULE N/A |
| 16. DISTRIBUTION STATEMENT (of this Report) Approved for public release; distribution unlimited. | | |
| 17. DISTRIBUTION STATEMENT (of the abstract entered in Block 20, if different from Report) <i>1. Tanks -- Insulation</i> <i>2. Insulation -- Performance</i> | | |
| 18. SUPPLEMENTARY NOTES Available in DDC. | | |
| 19. KEY WORDS (Continue on reverse side if necessary and identify by block number) space shuttles wind tunnel tests fuel tanks insulation materials | | |
| 20. ABSTRACT (Continue on reverse side if necessary and identify by block number) Aerothermal tests were conducted to evaluate the performance of a candidate material for the insulation of the Space Shuttle external tank. Material samples were exposed to total temperatures and heating rates designed to simulate those experienced during the ascent phase of the Shuttle trajectory. These conditions were obtained in the VKF Hypersonic Wind Tunnel (C), where a large wedge was used to hold the sample and the wedge angle was varied | | |

UNCLASSIFIED

UNCLASSIFIED

20. ABSTRACT (Continued)

to produce the desired heating rates and pressures on the wedge surface. Photographic coverage of the material performance was obtained at wedge angles from 0 to 38 deg. Selected test results are presented which show the ablation/erosion characteristics of the material.

UNCLASSIFIED

PREFACE

The work reported herein was conducted by the Arnold Engineering Development Center (AEDC), Air Force Systems Command (AFSC), at the request of the Marshall Space Flight Center (NASA/MSFC) for the Martin Marietta Co., Michoud Operations, under Program Element 921E. The results presented were obtained by ARO, Inc. (a subsidiary of Sverdrup & Parcel and Associates, Inc.), contract operator of AEDC, AFSC, Arnold Air Force Station, Tennessee, under ARO Project No. V41C-91A. The authors of this report were R. K. Matthews, ARO, Inc., and D. C. Harper, Captain, USAF. The data analysis was completed on March 17, 1975, and the manuscript (ARO Control No. ARO-VKF-TR-75-57) was submitted for publication on May 16, 1975.

CONTENTS

| | <u>Page</u> |
|--|-------------|
| 1.0 INTRODUCTION | 5 |
| 2.0 APPARATUS | |
| 2.1 Wind Tunnel | 5 |
| 2.2 Test Hardware | 6 |
| 2.3 Instrumentation | 7 |
| 3.0 PROCEDURES | |
| 3.1 Test Conditions | 8 |
| 3.2 Test Procedures and Data Reduction | 8 |
| 4.0 RESULTS AND DISCUSSION | 10 |
| 5.0 CONCLUDING REMARKS | 12 |
| REFERENCES | 12 |

ILLUSTRATIONS

Figure

| | |
|--|----|
| 1. VKF Tunnel C | 13 |
| 2. Photograph of Test Hardware | 14 |
| 3. Sketch of Test Hardware | 15 |
| 4. Illustration of Optical Data Coverage | 16 |
| 5. Illustration of Grid Line Projection System | 17 |
| 6. "Calibration" of Grid Line Projection System | 18 |
| 7. Typical Schlieren Photograph | 19 |
| 8. Comparison of Wind Tunnel Conditions and Flight Conditions | 20 |
| 9. Comparison of Heat-Transfer Data and Theoretical Calculations | 21 |
| 10. Summary of Test Environment as a Function of Wedge Angle | 22 |
| 11. Photographs Illustrating the Nonrepeatability of Sample Behavior | 23 |
| 12. Photographs Illustrating an Example of Groove Formation | 24 |
| 13. Photographs Illustrating Erosion of BX250 | 25 |
| 14. Photographs Illustrating Wedge Angle (i.e., \dot{q}_0) Effect | 26 |
| 15. Photographs Obtained During Trajectory C Run | 29 |
| 16. Photographs Illustrating the Lack of Erosion at $T_0 = 1080^\circ\text{F}$ | 30 |
| 17. Photographs Illustrating the Effect of a Protuberance on CPR 421 | 31 |
| 18. Schlieren Photograph of Flow Field Around Protuberance | 32 |

TABLES

1. Description of Material Samples 33

2. Test Summary 34

NOMENCLATURE 35

1.0 INTRODUCTION

The external tank of the Space Shuttle will contain liquid propellants, and the tank surface will be extremely cold if it is not insulated. This cold surface may collect frost or ice, which will add weight and may be dislodged during ascent, possibly damaging the surface of the orbiter. Therefore, to prevent a frost buildup on the external tank, an insulating covering has been proposed. This insulating cover should be as light as possible to minimize the adverse effect on payload weight but must also withstand the flight aerothermal environment. The objective of the present tests, requested by the National Aeronautics and Space Administration/Marshall Space Flight Center (NASA/MSFC), was to evaluate the performance of a candidate material in an environment simulating that of the ascending shuttle vehicle. The material proposed by Martin Marietta Co., the prime contractor for the tank, is known as CPR 421.

The tests were conducted in the von Kármán Gas Dynamics Facility (VKF) Hypersonic Wind Tunnel (C), which is a continuous flow, Mach 10 wind tunnel. Material samples were exposed to stagnation temperatures and local heating rates designed to simulate those experienced during the ascent phase of the Shuttle trajectory. These conditions were obtained by using a variable wedge angle to produce the desired heating rates.

Photographic coverage of the material performance was obtained at wedge angles from 0 to 38 deg. In addition to the photographic data, pressure and heat-transfer-rate measurements were made to experimentally verify the predicted flow conditions. Boundary-layer trips were positioned near the leading edge of the wedge to provide a turbulent boundary layer. The vast majority of the tests were conducted at a flow total temperature of 1900°R (1440°F); however, some data were also obtained at a total temperature of 1540°R (1080°F).

2.0 APPARATUS

2.1 WIND TUNNEL

Tunnel C (Fig. 1) is a continuous, closed-circuit, variable density wind tunnel with an axisymmetric contoured nozzle and a 50-in.-diam test section. The tunnel operates at a nominal free-stream Mach number of 10 at stagnation conditions from 200 to 2000 psia at 1900°R. A model may be injected into the tunnel for a test run and then retracted for model cooling or model changes without interrupting the tunnel flow. A description of the tunnel may be found in Ref. 1.

Normally this tunnel is used for hypersonic aerodynamic testing of scaled models of aerospace vehicles. For the present tests, aerodynamic convective heating rates and total

temperature were the primary test conditions required to simulate the flight environment. The test technique, developed at VKF to accommodate these requirements, utilized a large wedge which was used to process the tunnel free-stream flow through an oblique shock. The flow conditions behind the oblique shock and on the surface of the wedge where the material sample was placed were tailored by varying wedge angle and tunnel free-stream conditions to provide the needed test parameters.

2.2 TEST HARDWARE

The majority of the test samples were 14- by 17- by 1-in. slabs of Isonate® CPR 421 sprayed on a thin sheet of Aluminum. CPR 421 is a product of the UpJohn Company, Torrance, California, and is a cellular foam with a density of about 2.0 lbm/ft³. The two components utilized to produce CPR 421 belong to the following chemical families:

Component A - Isocyanate, chloroalkyl phosphate ester

Component B - Polyol resin, helocarbon

Besides the CPR 421 samples, one BX 250 sample and three SLA 561 samples were tested. All the samples were provided by the Martin Marietta Company, New Orleans, Louisiana.

A representative pretest photograph of a CPR 421 test sample installed on the wedge is shown in Fig. 2, and a list describing the test samples is presented in Table 1.

A sketch of the wedge is shown in Fig. 3. The basic wedge was the same as that described in Ref. 2, with a few modifications so that material samples could be tested. The wedge angle was 33.65 deg; however, during the current test offset stings were used in conjunction with the model pitch mechanism, which provided for wedge angles from 0 to 38 deg. In addition to the material samples a steel "calibration plate" was fabricated with pressure tubes and heat-rate gages installed. The location of this instrumentation is also illustrated in Fig. 3. Spacer plates were installed to position the top surface of the samples or "calibration plate" level with the forward portion of the wedge.

Since there will be a turbulent boundary layer on the Shuttle external tank during actual flight, it was necessary to provide a turbulent boundary layer during the wind tunnel test. This was accomplished by installing three rows of "trip" spheres 3 in. from the leading edge of the wedge. The trip sphere diameters were 0.032 in. for the first entry and 0.047 in. for the second and third entries. The details of the trip sphere installation are also illustrated in Fig. 3.

2.3 INSTRUMENTATION

The primary data consisted of 70-mm sequenced photographs taken with a camera mounted on top of the tunnel (see Fig. 4). The camera used Kodak® TRI-X Pan black-and-white film, and the time from the start of model injection to each picture was recorded on magnetic tape. The camera was operated at a nominal rate of one frame every two seconds; however, toward the end of each run the frame rate was decreased to conserve film.

In addition to the primary data, backup data were obtained with a 16-mm motion picture camera, and "instant replay" capability was provided by video taping each run (see Fig. 4). The motion picture camera was operated at 24 frames per second and used Kodak Ektachrome EF color film. The "instant replay" capability simplified decision making during the test and significantly increased the efficiency of the operation.

The photographs provided excellent qualitative data; however, quantitative results were also desired. These were provided by a unique grid line projection system, which is illustrated in Fig. 5. A standard slide projector was mounted on top of the tunnel, and a slide was made such that grid lines spaced about 2 in. apart were projected onto the sample at an acute angle. As the material surface receded, the projected lines appeared to translate toward the leading edge as viewed from the position of the 70-mm camera.

This system was calibrated for each wedge angle and camera installation by photographing a sample level with the wedge surface and then removing a known thickness of spacers and again photographing the sample. Two typical calibration photographs are presented in Fig. 6a. An enlarger was used to measure the translation of each grid line so that "scale factors" (S.F.) could be determined. The scale factor is defined as follows:

$$S.F. \equiv \frac{\left(\frac{\text{Inches of Translation}}{\text{Inches of Recession}} \right)}{\left(\begin{array}{c} \text{Span at Interface of} \\ \text{Sample and Wedge} \\ \text{for Particular Photograph} \\ \text{Being Used} \end{array} \right)} \quad (1)$$

A summary of these scale factors is presented in Fig. 6b.

The material recession scale shown on several figures in this report indicates the grid line translation distance, which corresponds to a 1-in. recession of the sample material. This scaled distance was obtained by measuring the wedge span for the specific pictures and using the scale factors presented in Fig. 6b. That is,

$$(\text{Grid Line Translation}/1\text{-in. Recession}) = (S.F.)(\text{Span as Measured})$$

The measurement of translation distance between an early picture and a later picture is made easier by the side-to-side alignment of these pictures.

The two wedge pressures (see Fig. 3) were measured with 1- and 15-psid transducers which were switched in and out of the system automatically to allow measuring to the best precision. All transducers were referenced to a near vacuum. From repeat calibrations, the estimated precision was ± 0.001 psia or ± 0.5 percent, whichever was greater. Model flow-field schlieren photographs were obtained during all tests. Figure 7 shows a typical photograph.

Heat-transfer rates were measured with gages installed at five locations on the wedge surface. The location of the gages (see Fig. 4) provided for both axial and spanwise heating distributions. A description of these high sensitivity gages and their applications is presented in Ref. 3.

3.0 PROCEDURES

3.1 TEST CONDITIONS

The nominal free-stream test conditions are listed below.

| M_∞ | p_o , psia | T_o , °R | H_o , Btu/lbm |
|------------|--------------|------------|--------------------|
| 10 | 1800 | 1900 | 475 |
| 10 | 1800 | 1540 | 375 |

A complete test matrix is presented in Table 2.

3.2 TEST PROCEDURES AND DATA REDUCTION

One of the first things that was determined during the test was the specific aerodynamic conditions on the wedge surface. Pressure and heat-transfer data were obtained by use of the instrumented "calibration plate" (see Fig. 3). The heat-transfer data were obtained by injecting the wedge into the tunnel and recording the millivolt output of the heat gages on magnetic tape. The heat-transfer rate as measured by the gage was computed as

$$\dot{q} = (CF) (\Delta E) \quad (2)$$

where

ΔE is the millivolt output and

CF is the gage calibration factor

The calibration factor for each gage was obtained by direct measurement of the gage output for a known heating rate input. These calibrations were performed by personnel of the VKF Instrumentation Branch.

The conversion from heating rate to Stanton number was accomplished as follows:

$$St_{\infty} = \frac{\dot{q}}{\rho_{\infty} V_{\infty} C_p (T_o - T_w)} \quad (3)$$

where

ρ_{∞} = Free-stream air density

V_{∞} = Free-stream velocity

C_p = Specific heat (~ 0.256 for present conditions)

T_o = Measured tunnel stagnation temperature* ($^{\circ}R$)

T_w = Effective wall temperature of gage,
($T_w = T_G + 0.75\Delta T$) where $\Delta T = (K)(\Delta E)$

The temperature adjustment for T_w accounts for the temperature gradient across the gage surface since the center of the gage was at a slightly higher temperature than the outer case temperature. The precision of the heating rates determined from the Gardon gages is estimated to be ± 5 percent.

One parameter which has been used by Martin Marietta and NASA/MSFC to correlate insulation material recession data is the heating rate that corresponds to a wall temperature of $0^{\circ}F$ ($460^{\circ}R$). Of course, the wall temperatures during the test were significantly higher than this; therefore, \dot{q}_o was calculated as follows:

$$\dot{q}_o = St_{\infty} \rho_{\infty} V_{\infty} C_p (T_o - 460^{\circ}R) \quad (4)$$

where $T_w = 0^{\circ}F$ (i.e. $460^{\circ}R$), and the other parameters are defined above. Figure 8 is a plot of this parameter versus time for a specific location on the external tank and for a representative ascent trajectory. This anticipated thermal environment was provided by Rockwell International (RI).

*Normally the recovery temperature is used; however, since determination of this parameter requires some assumptions, it has become common to substitute T_o (a measured parameter).

The procedures used for testing the samples can be categorized as

1. Constant wedge angle runs
2. Variable wedge angle runs

For the constant wedge angle runs the samples were installed on the wedge and injected into the airstream at the desired wedge angle to provide a specified value of \dot{q}_0 . Photographic data were obtained for the duration of the run.

The variable wedge angle runs were intended to simulate the actual ascent trajectory of the external tank in terms of the thermal environment (i.e., \dot{q}_0 values).

4.0 RESULTS AND DISCUSSION

During this test, material samples were subjected to a relatively severe aerothermodynamic environment. Determination of this environment was an important part of the test. Measured Stanton number distributions are compared with laminar and turbulent calculations in Fig. 9. As can be seen there is excellent agreement between the data and the turbulent theory for $\theta_w \geq 9$ deg. For $\theta_w = 0$ and 6 deg the data imply that a transitional boundary layer was present. Heating rates calculated from these data [see Eq. (4)] are presented in Fig. 10a, and values obtained from this figure will be used as the correlating parameter in the remainder of this report. This figure also indicates that the wedge flow was two-dimensional since there were no significant trends in the spanwise data. Model surface pressure data at various wedge angles are shown in Fig. 10b.

The photographs presented in Fig. 11 represent typical data obtained during test runs. These three photographs were obtained at 40 sec of exposure to the airflow, and the flow conditions were identical for the three runs. As can be seen, irregular grooves (distorted grid lines) have been produced at various locations on the samples. In the regions where grooves did not form, the recession was negligible. The basic conclusions that can be made from examination of these data are (1) the ablation/erosion characteristics of the samples were nonrepeatable from sample to sample and (2) erosion characteristics cannot be directly correlated by aerothermodynamic parameters alone (i.e., \dot{q} , p_w , etc.) since the flow field was uniform and the erosion was not uniform.

Another example of groove formation is presented in Fig. 12. The top and bottom photographs were obtained at run times of 62 and 67 sec, respectively. Although there was only 5 sec between pictures, during this time a large groove formed down the middle of the sample. Conversely, the groove on the right did not change significantly in the 27 sec of elapsed time between the top picture of Fig. 11 and the bottom picture of

Fig. 12 (same run). The implication is that the grooving phenomenon is linked directly to the structural characteristics of the sample material.

Figure 13 presents photographs obtained with a different sample material. This material is known as BX250, and although "grooves" did not occur, it can be seen that the entire thickness (≈ 1 in.) of the sample has eroded away in only 36 sec. Clearly CPR 421 is more durable than BX250.

Figures 14a through c illustrate the influence of increased wedge angle (or \dot{q}) on the erosion characteristics of CPR 421 samples. It should be pointed out that in the right-side pictures the exposure times are not all the same; therefore, direct comparisons should not be made. However, it is clear that for $\theta_w = 9$ deg (Fig. 14a) the erosion after 150 sec was insignificant, whereas for $\theta_w = 38$ deg (Fig. 14c) there was about 0.3 in. of erosion in only 12 sec. It is also interesting to note that in the left-hand picture of Fig. 14c there is a strip of sample material that has not eroded. Posttest inspection of the wedge revealed that the trip spheres had been blown off at this spanwise location. The implication is that the flow was laminar over this part of the material and that the erosion for a laminar boundary layer is less than that for a turbulent boundary layer.

The preceding figures were for runs with a constant wedge angle. The results of a variable wedge angle run are presented in Fig. 15. The wedge angle was varied with time to simulate the heating rates predicted during actual flight.* For flight conditions, a turbulent boundary layer will exist during the majority of the trajectory, whereas in the tunnel a turbulent boundary layer was known to exist for only 50 sec of the 600-sec run. Thus it should not be assumed that these data are directly applicable to a 600-sec flight trajectory.

Perhaps the most positive result of the test is illustrated in Fig. 16, which presents photographs from a constant wedge angle ($\theta_w = 23$ deg) run with a total temperature of 1540°R . The photographs show no signs of erosion even after an exposure time of 99 sec. Comparison of these results with those of the previous figures ($T_o = 1900^\circ\text{R}$) implies that there is a total temperature below which ablation/erosion will not be significant. An important qualification on this statement is presented in the next figure.

Figure 17 illustrates the severe local erosion that can occur in the vicinity of protuberances. The protuberance in this case was a 1-in.-diam vertical cylinder which extended about 0.9 in. above the sample material. The interference flow field caused by this protuberance was sufficient to erode completely through the 1-in.-thick layer of CPR

*Flight was designated trajectory C for this test (see Fig. 8).

421 in only 4 sec (left-hand picture, Fig. 17). This flow field is shown in the schlieren photograph presented in Fig. 18.

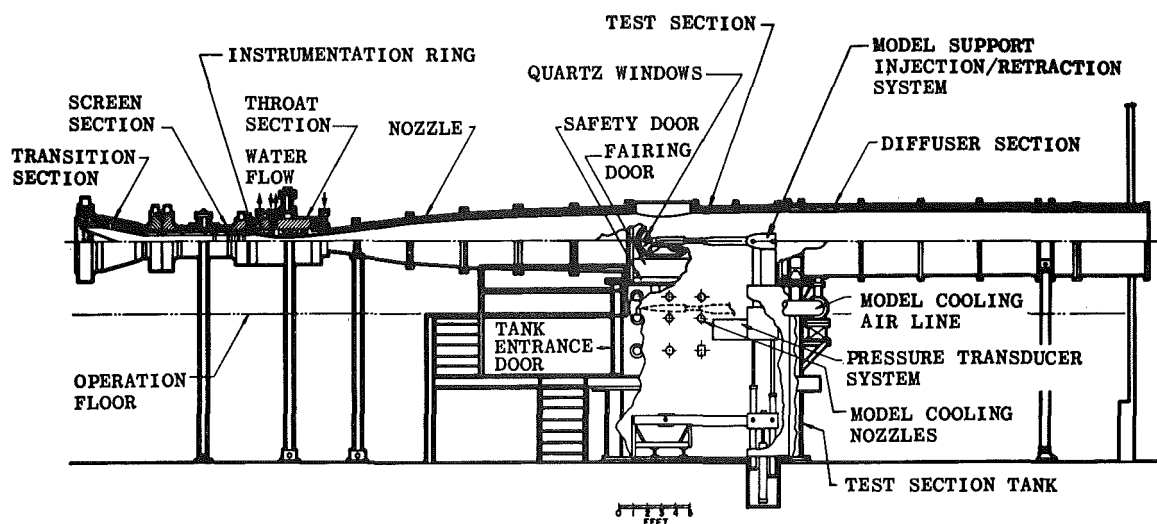
5.0 CONCLUDING REMARKS

Sample slabs of proposed insulation materials for the external tank of the space shuttle were tested under simulated flight conditions in the VKF 50-in.-diam Hypersonic Wind Tunnel (C). Photographic data recorded the ablation/erosion characteristics of the samples for a range of heating rates from 1 to 15 Btu/ft²-sec. A limited amount of data was obtained at a reduced total temperature of 1540°R and also with a protuberance on the sample. Based on these data the following conclusions can be drawn:

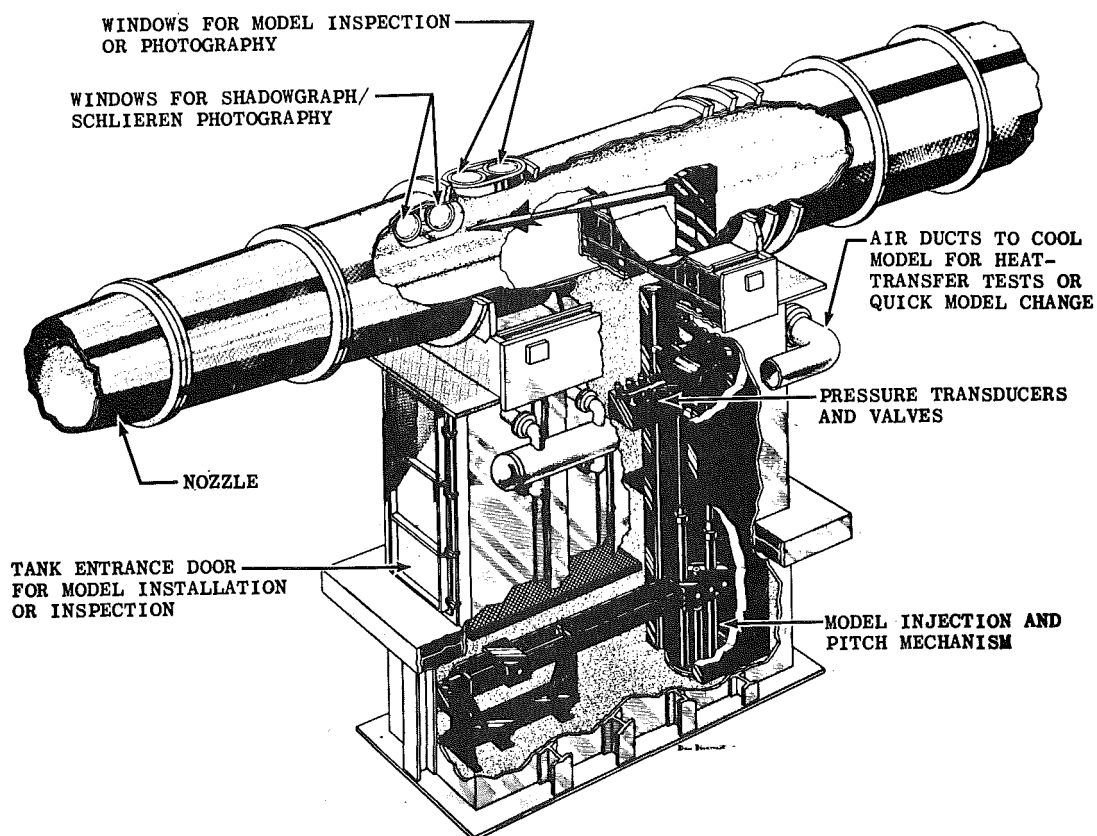
1. The CPR 421 erosion characteristics are nonrepeatable from sample to sample.
2. Local erosion characteristics cannot be directly correlated by aerothermodynamic parameters (i.e., \dot{q} , p , etc.) since the flow field is uniform and the erosion is not uniform.
3. CPR 421 is more durable than BX250.
4. For samples without a protuberance there is a total temperature between 1500 and 1900°R below which erosion will not be significant.
5. The interference flow field caused by a 1-in.-diam protuberance is sufficient to erode completely through a 1-in.-thick layer of CPR 421 in only 4 sec.

REFERENCES

1. Sivells, J. C. "Aerodynamic Design and Calibration of the VKF 50-Inch Hypersonic Wind Tunnels." AEDC-TDR-62-230 (AD299774), March 1962.
2. Matthews, R. K. "Experimental Investigation of Water Ejection from a Wedge Model at Mach Number 6." AEDC-TR-71-26 (AD721448), April 1971.
3. Trimmer, L. L., Matthews, R. K., and Buchanan, T. D. "Measurement of Aerodynamic Heat Rates at the von Kármán Facility." ICIASF 1973: Record of International Congress of Instrumentation in Aerospace Simulation Facilities, September 1973.
4. Harms, R. J., Schmidt, C. M., Hanawalt, A. J., and Schmitt, D. A. "A Manual for Determining Aerodynamic Heating of High-Speed Aircraft." Bell Aircraft Corporation, Report No. 7006-3352-001 (AD229434), June 1959.



a. Tunnel assembly



b. Test section

Figure 1. VKF Tunnel C.

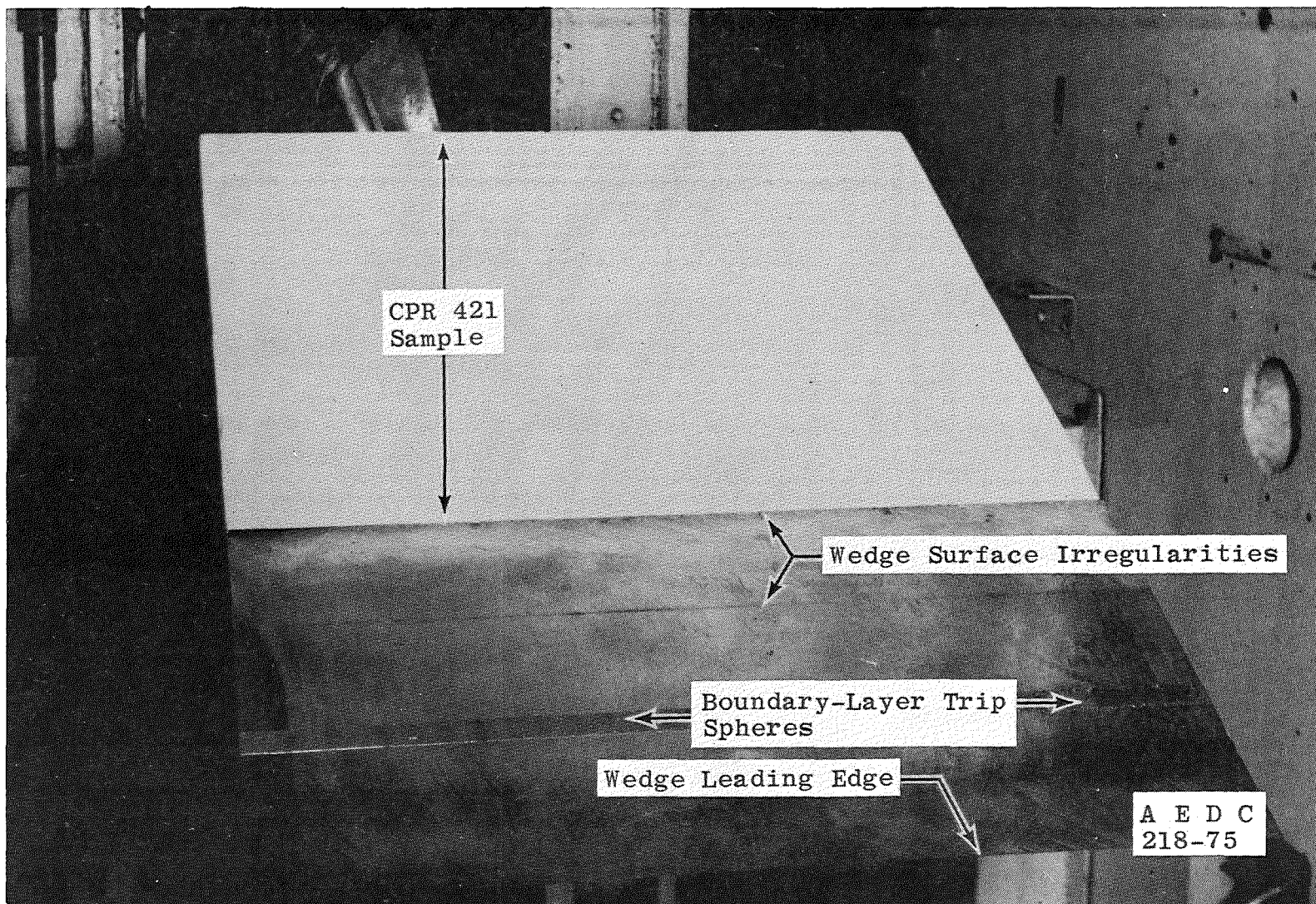


Figure 2. Photograph of test hardware.

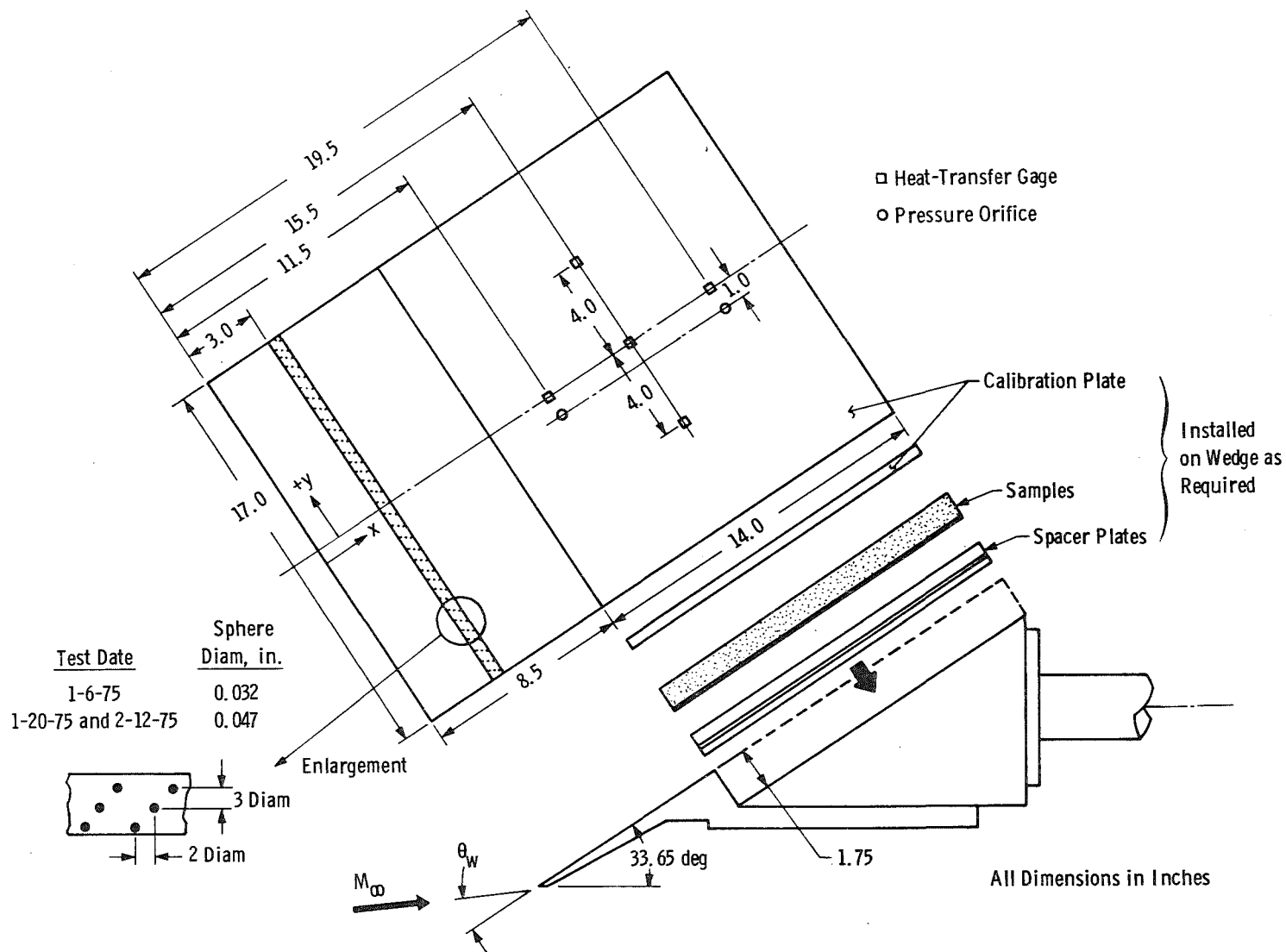


Figure 3. Sketch of test hardware.

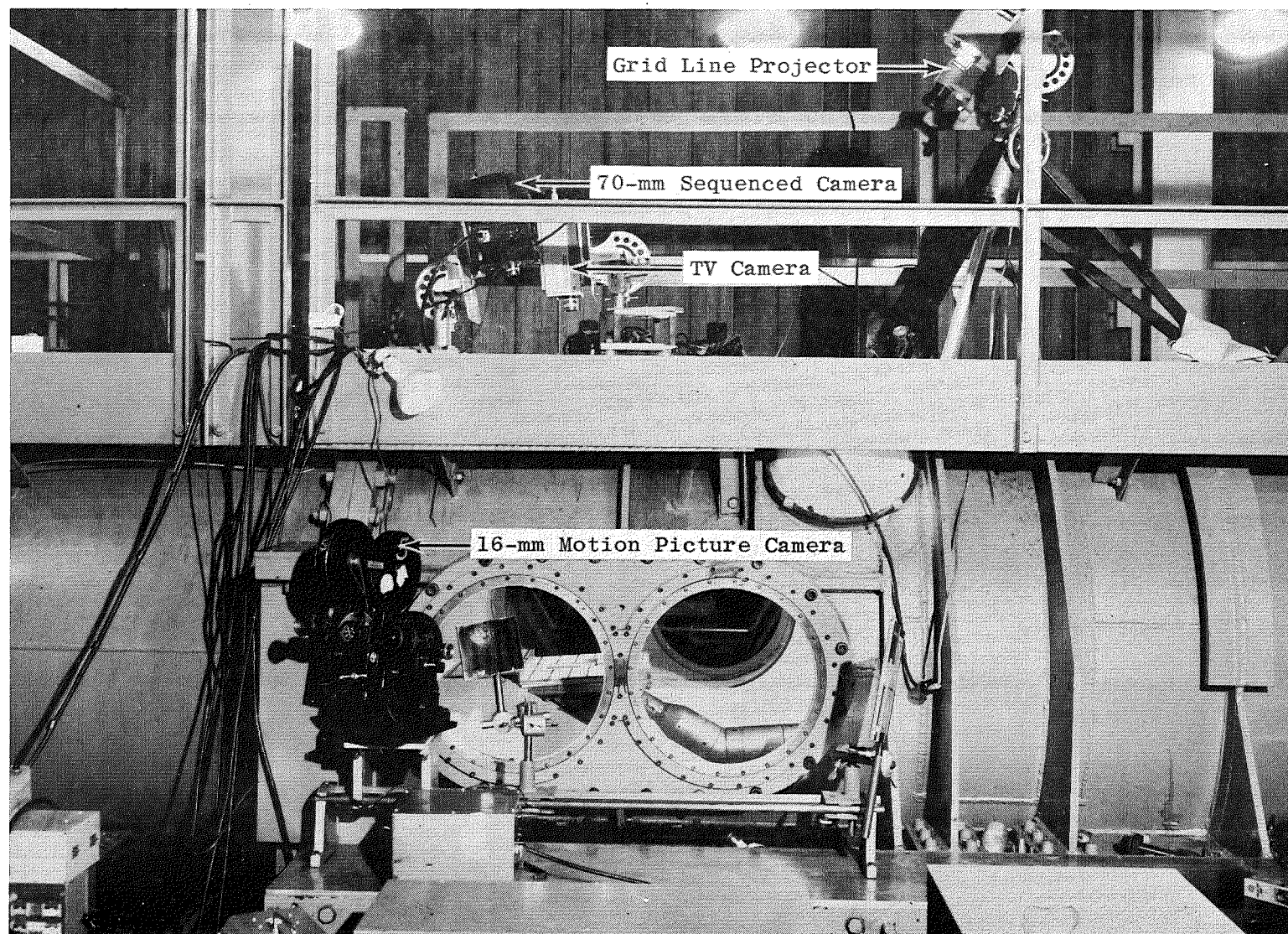


Figure 4. Illustration of optical data coverage.

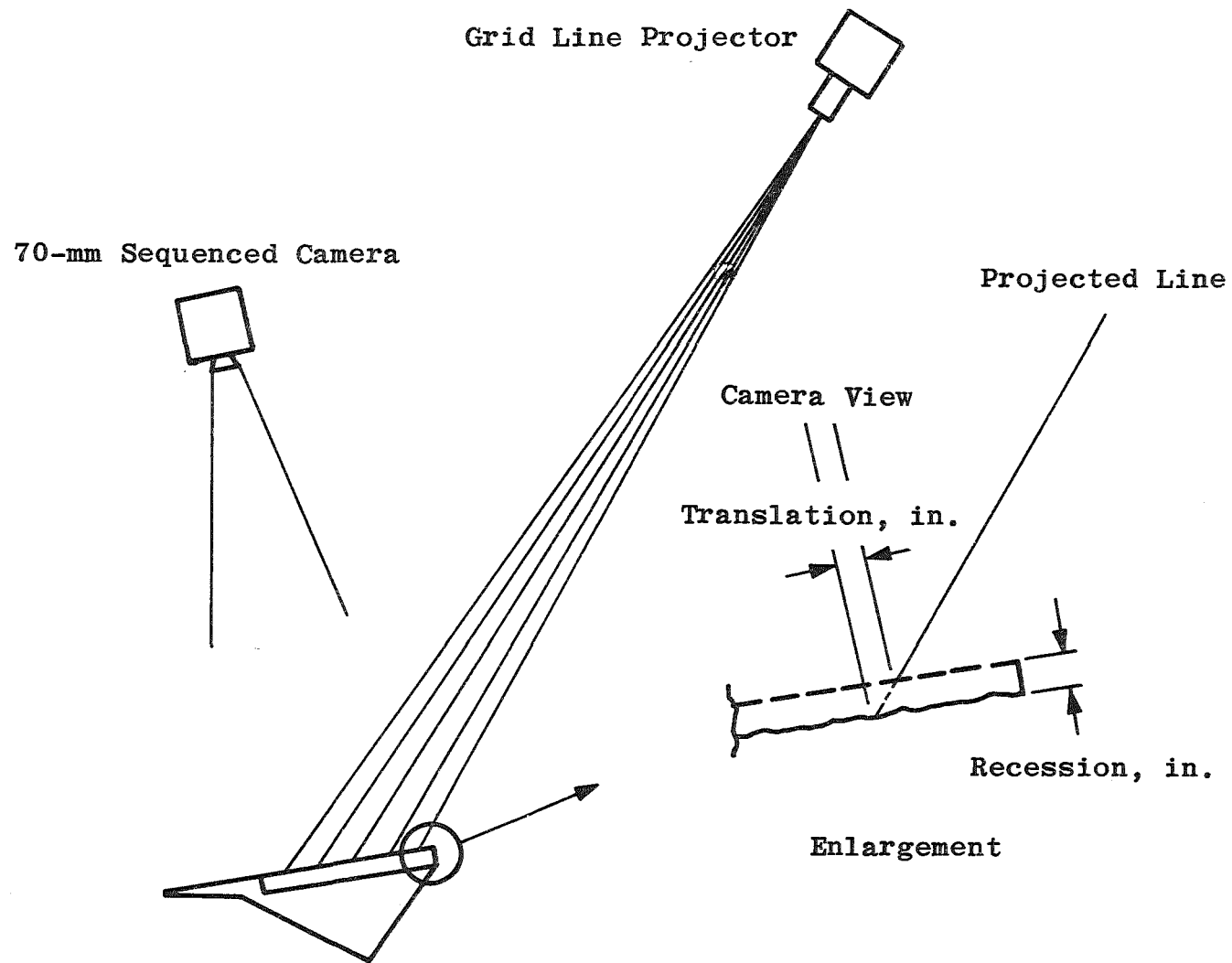
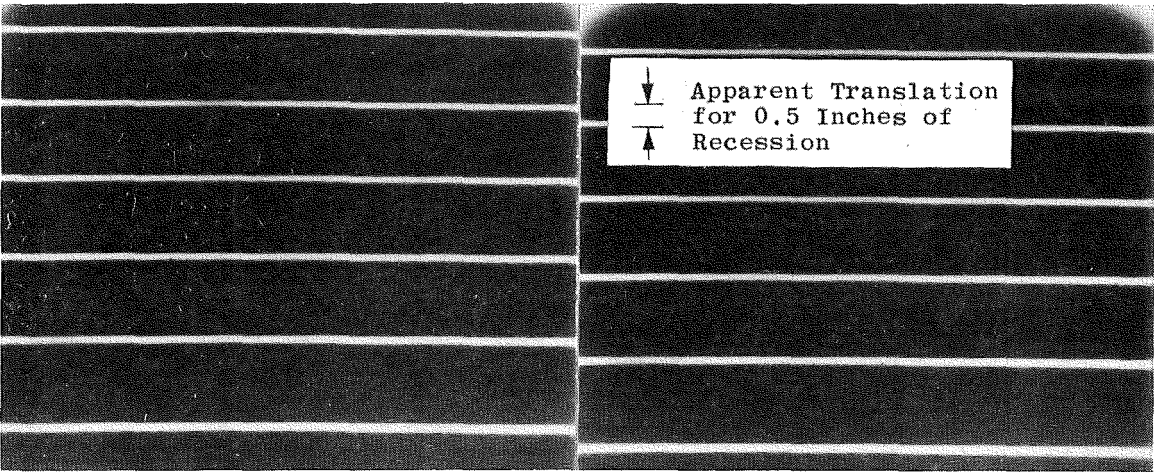


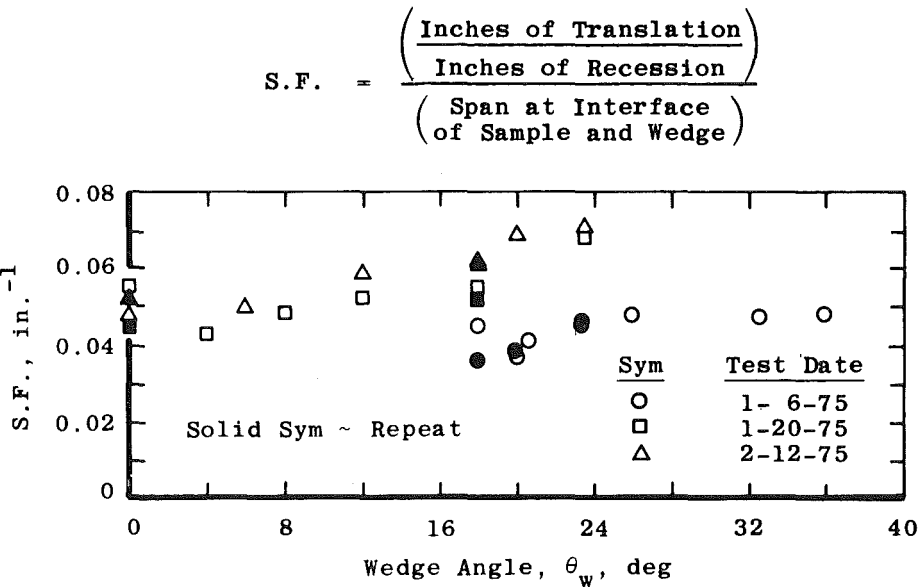
Figure 5. Illustration of grid line projection system.



$\theta_w = 12$
Surface Level with Wedge

$\theta_w = 12$
Surface Recessed 0.5 in.

a. Grid system "calibration" photographs



b. Scale factors

Figure 6. "Calibration" of grid line projection system.

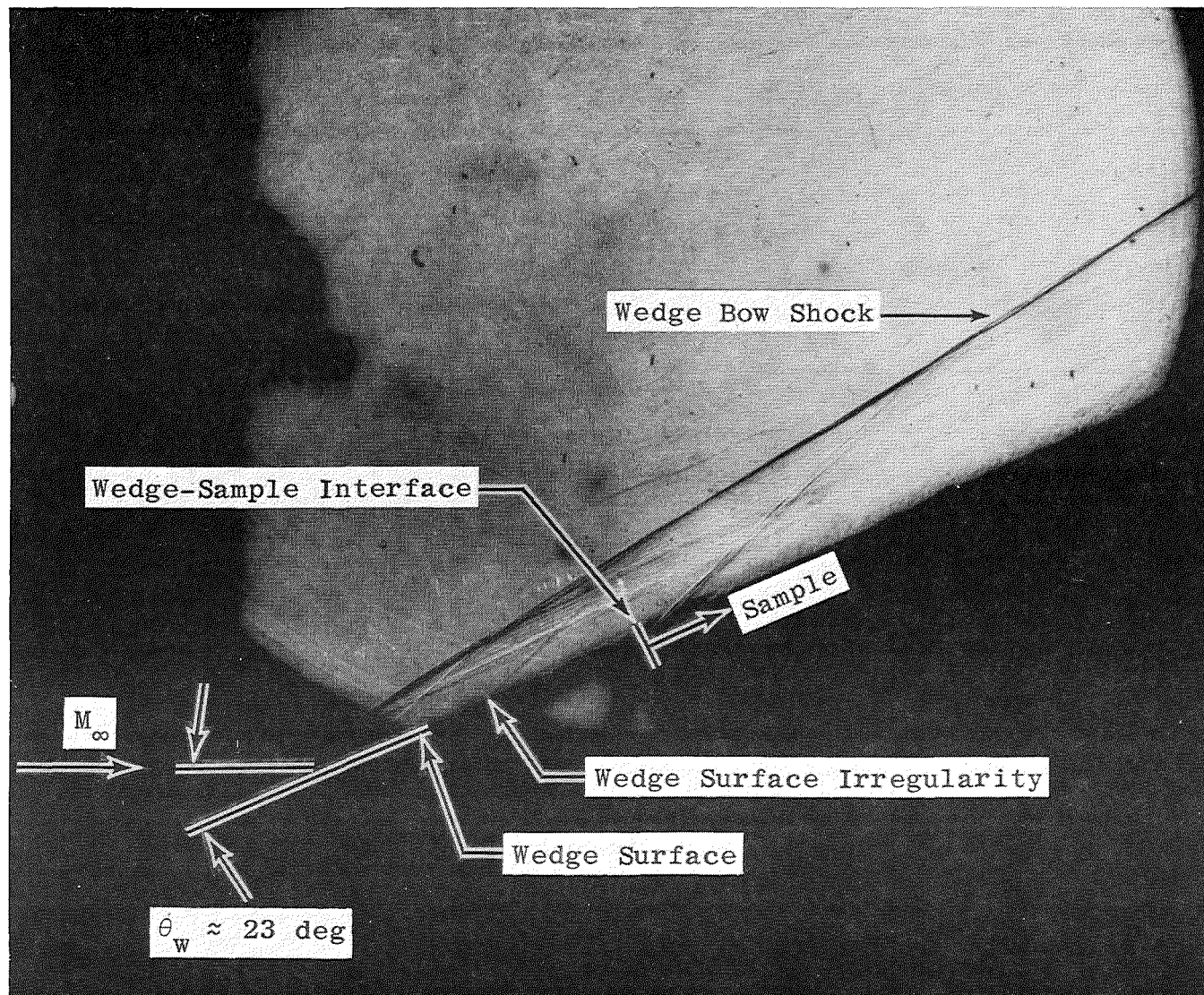


Figure 7. Typical schlieren photograph.

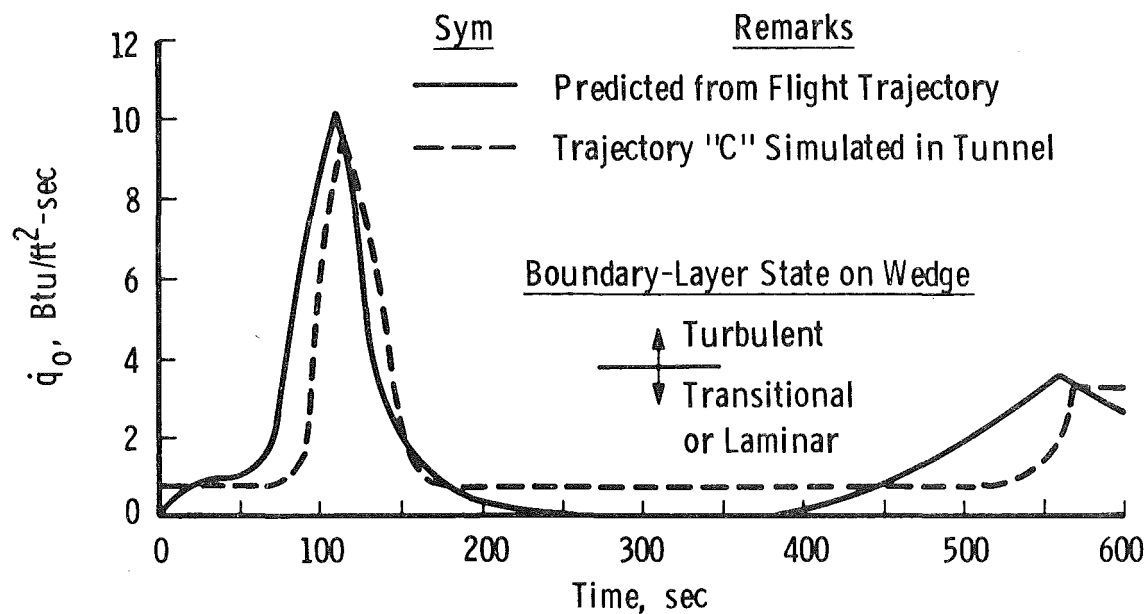
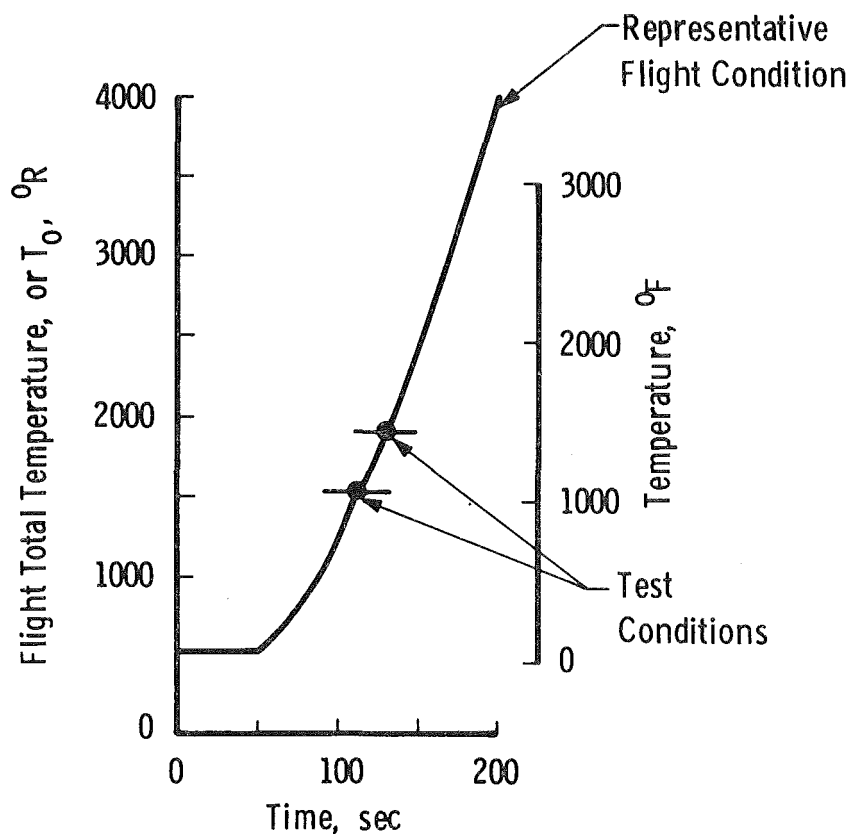


Figure 8. Comparison of wind tunnel conditions and flight conditions.

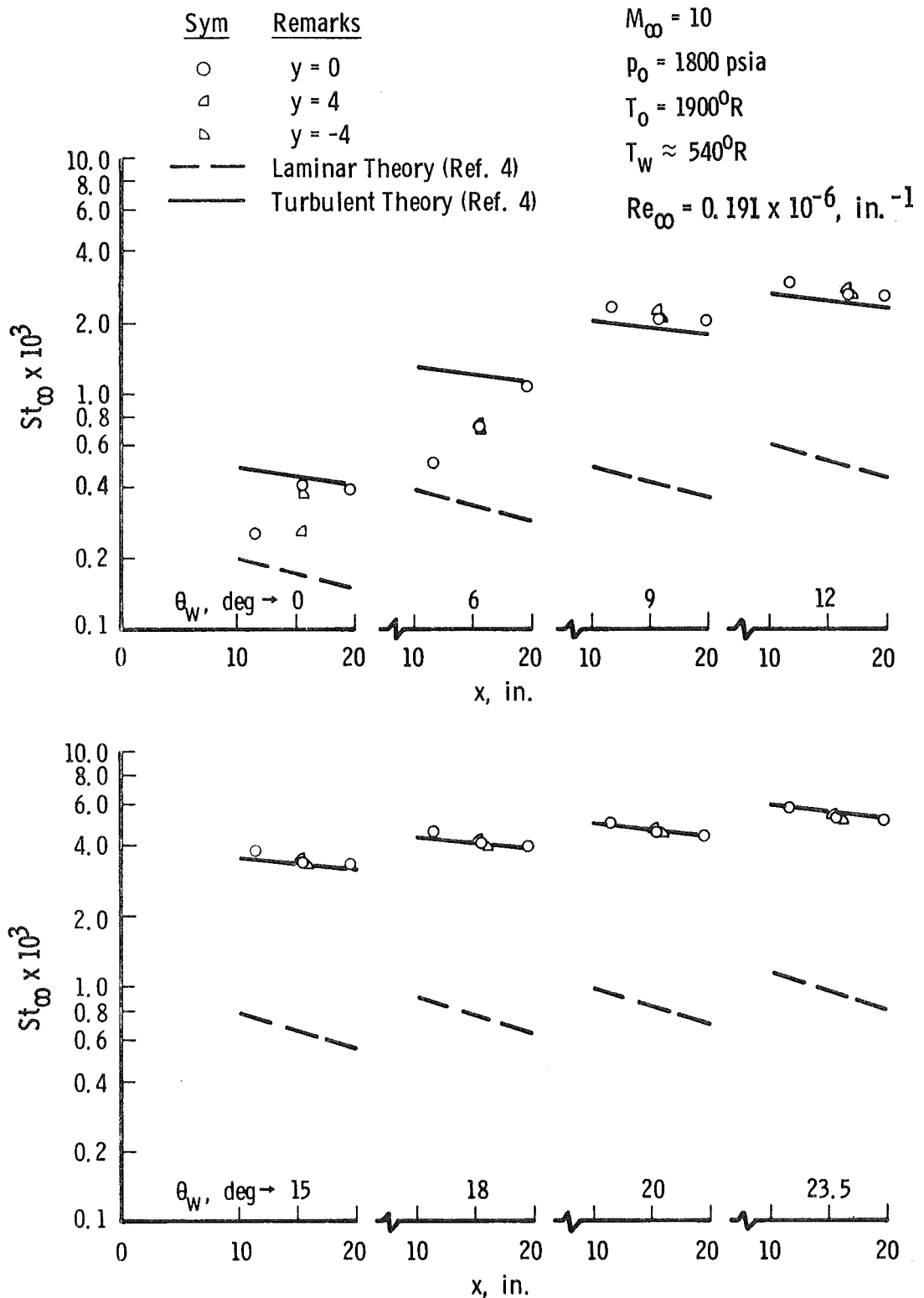


Figure 9. Comparison of heat-transfer data and theoretical calculations.

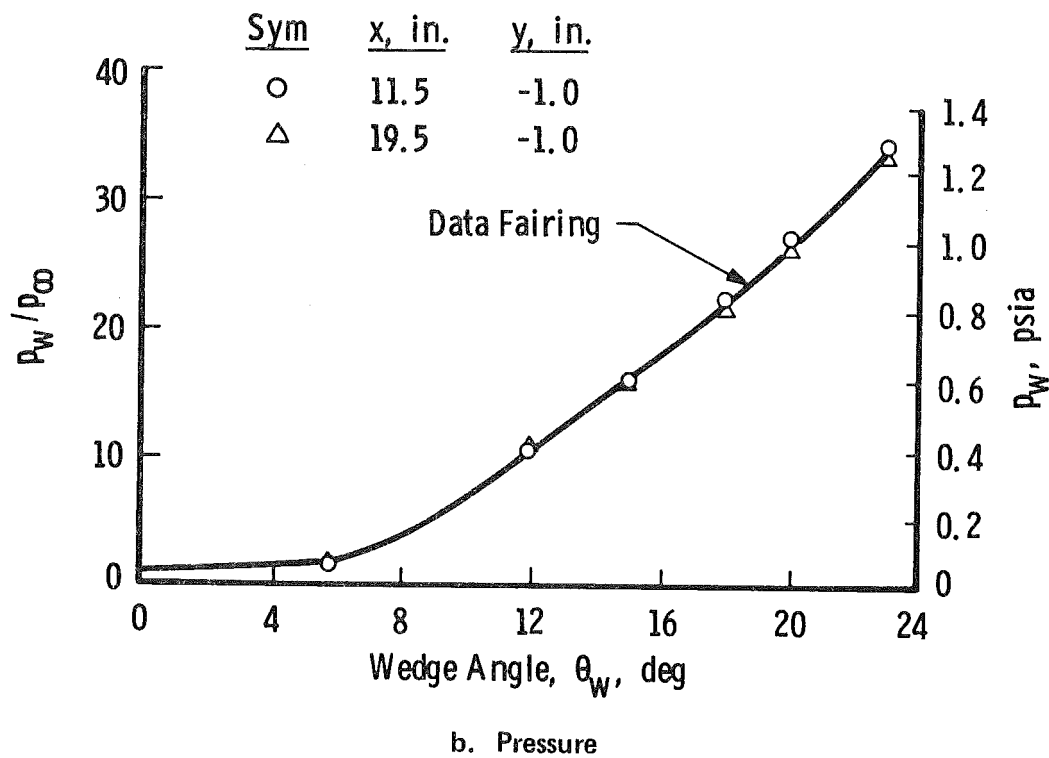
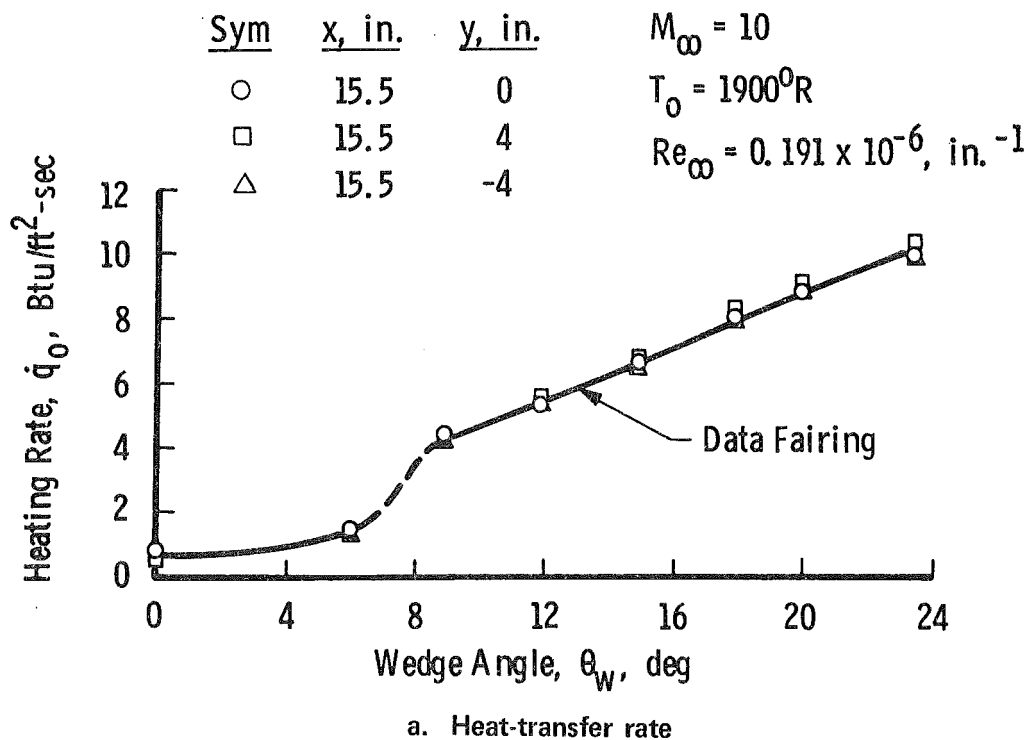


Figure 10. Summary of test environment as a function of wedge angle.

Pictures Taken from Different Runs with Identical Conditions

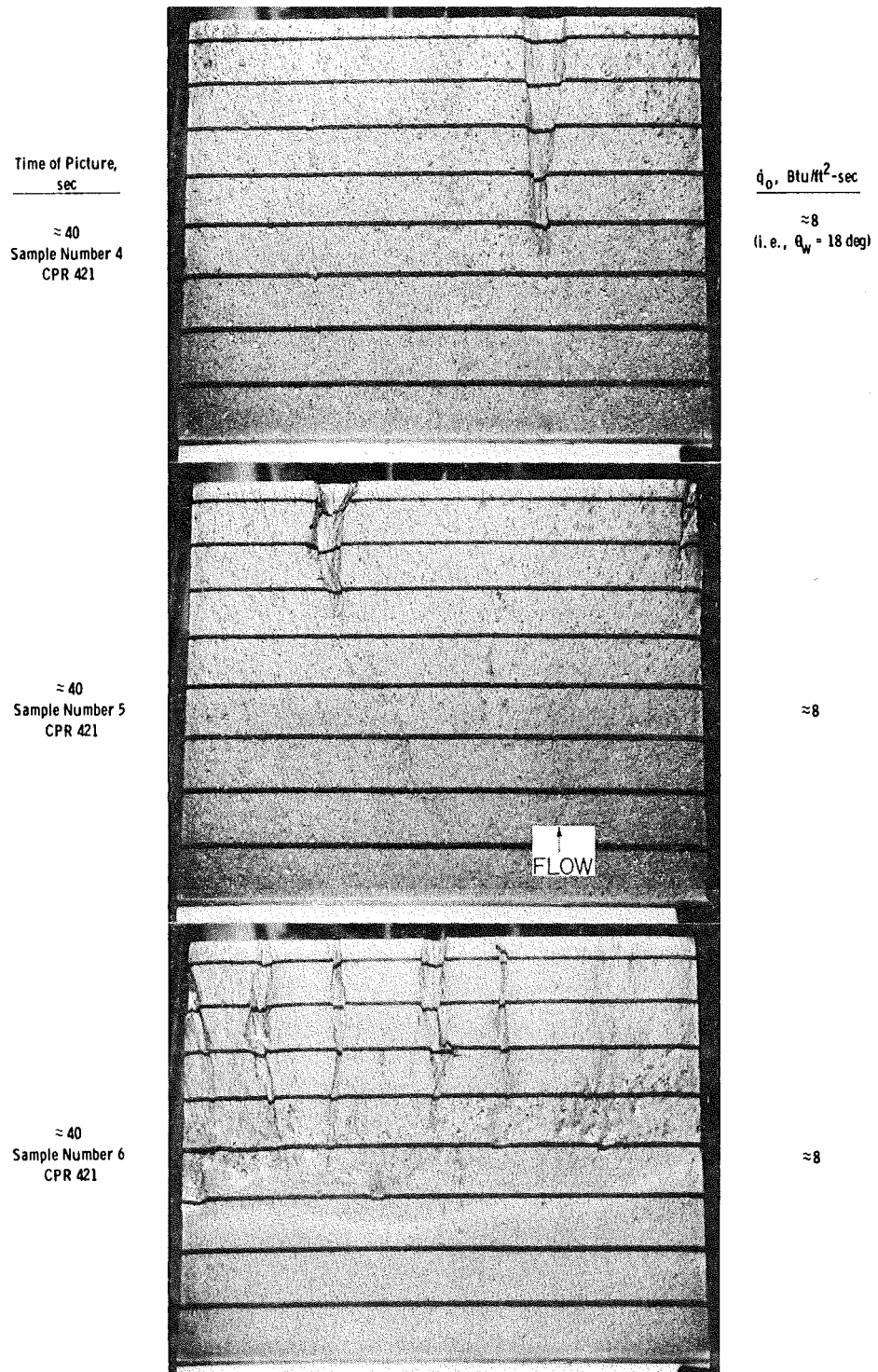
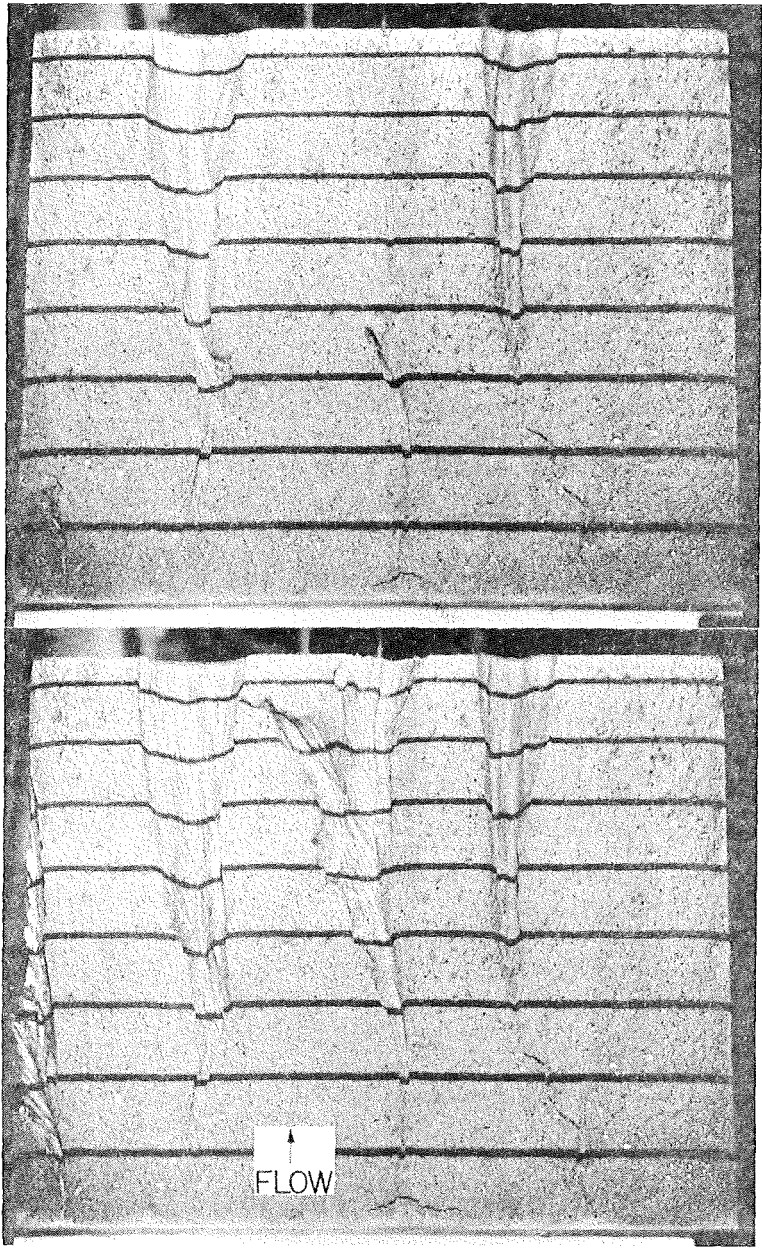


Figure 11. Photographs illustrating the nonrepeatability of sample behavior.

Note: Time between pictures was only 5 sec.
This run is same as that of top picture in Figure 11.

Sample Number 4
Time of Picture,
sec

≈ 62
CPR 421

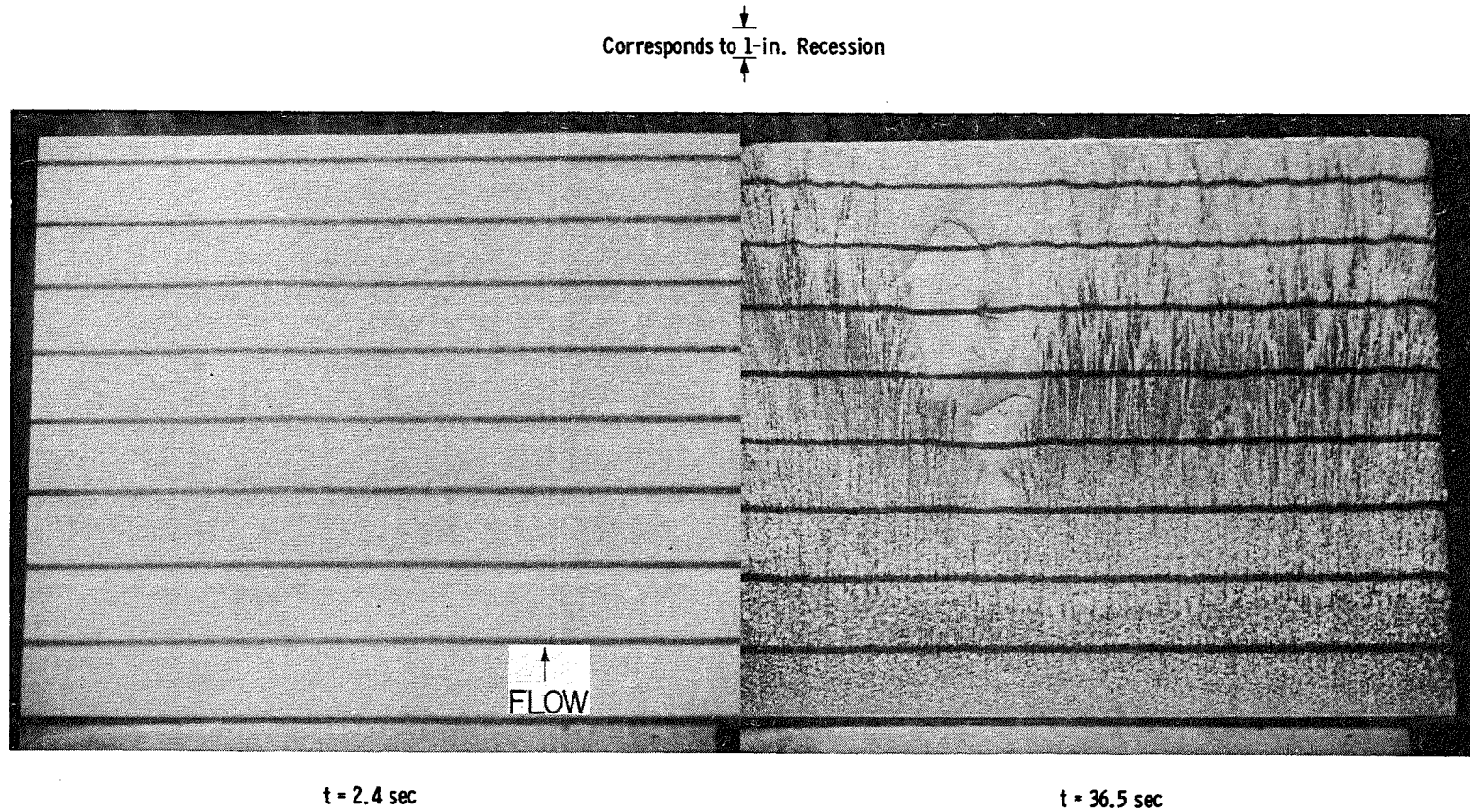


\dot{q}_0 , Btu/ft²-sec

≈ 8

≈ 8

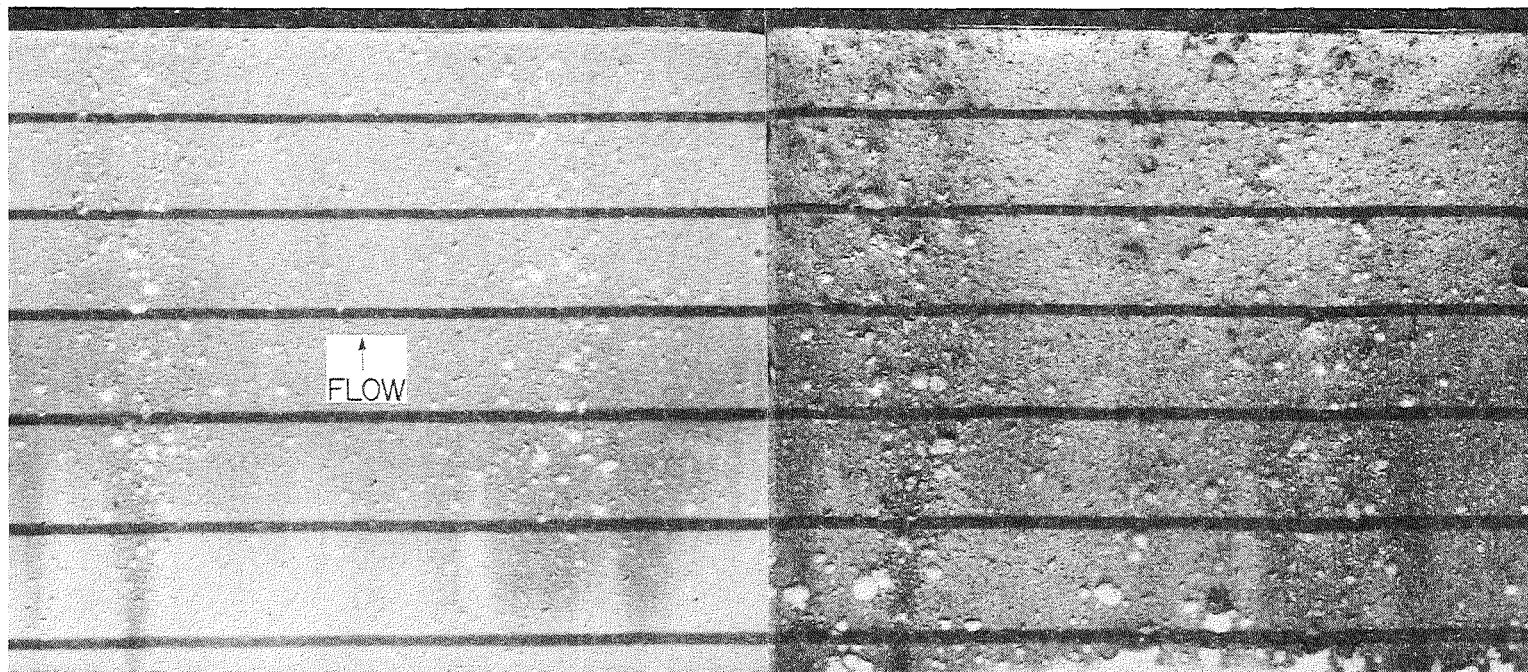
Figure 12. Photographs illustrating an example of groove formation.



Sample No. 101: $\theta_w = 18 \text{ deg}$, $\dot{q}_0 \approx 8 \text{ Btu/ft}^2\text{-sec}$

Figure 13. Photographs illustrating erosion of BX250.

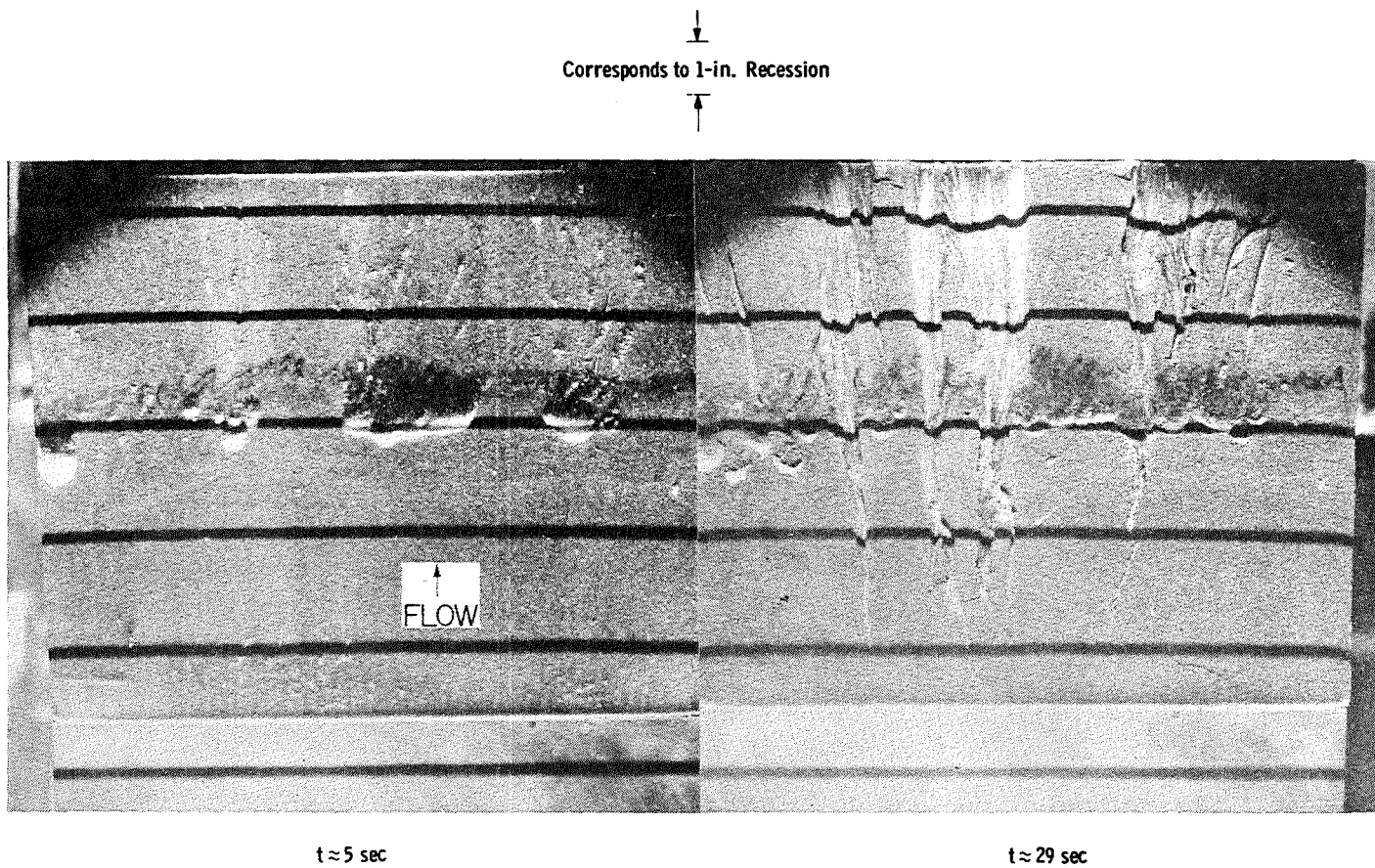
Corresponds to 1-in. Recession



$t \approx 6 \text{ sec}$

$t \approx 150 \text{ sec}$

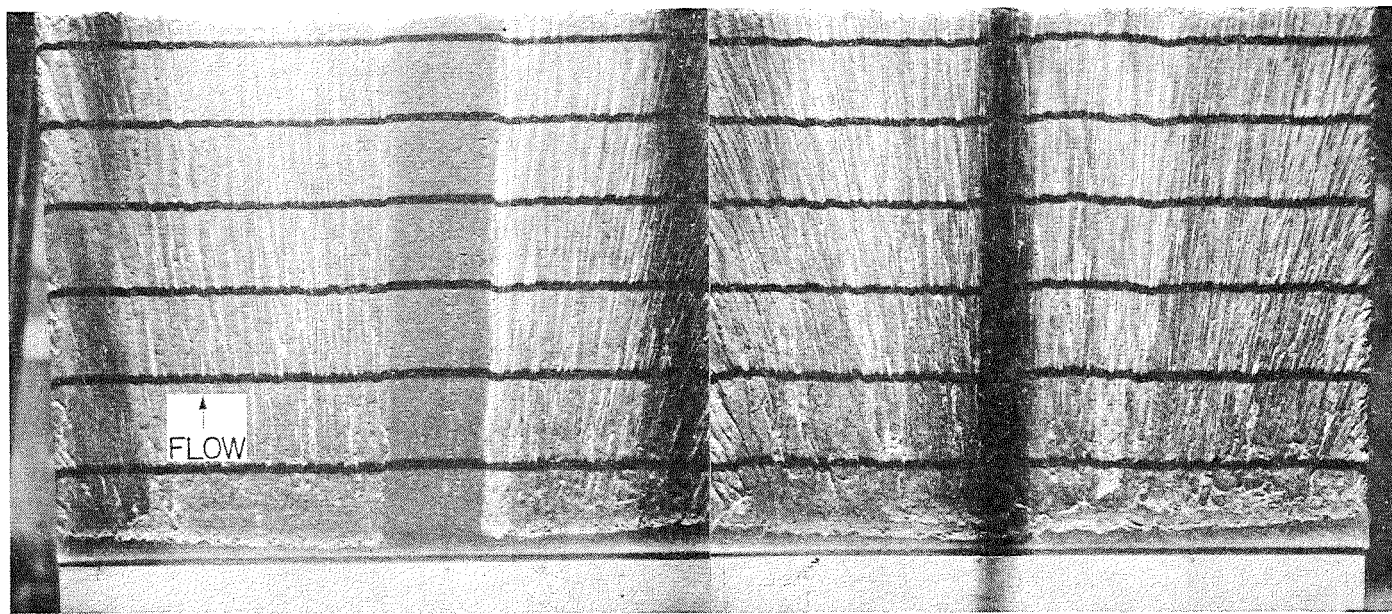
a. $\theta_w = 9 \text{ deg}$ ($\dot{q}_o = 4.3 \text{ Btu/ft}^2\text{-sec}$), sample No. 29, CPR 421
 Figure 14. Photographs illustrating wedge angle (i.e., \dot{q}_o) effect.



b. $\theta_w = 23.5 \text{ deg}$ ($\dot{q}_o = 10 \text{ Btu/ft}^2\text{-sec}$), sample No. 24, CPR 421
Figure 14. Continued.

Note: The value of \dot{q}_0 for $\theta_w = 38$ deg was obtained by extrapolation of the data of Fig. 10.

Corresponds to $\frac{1}{2}$ -in. Recession



$t \approx 5$ sec

$t \approx 12$ sec

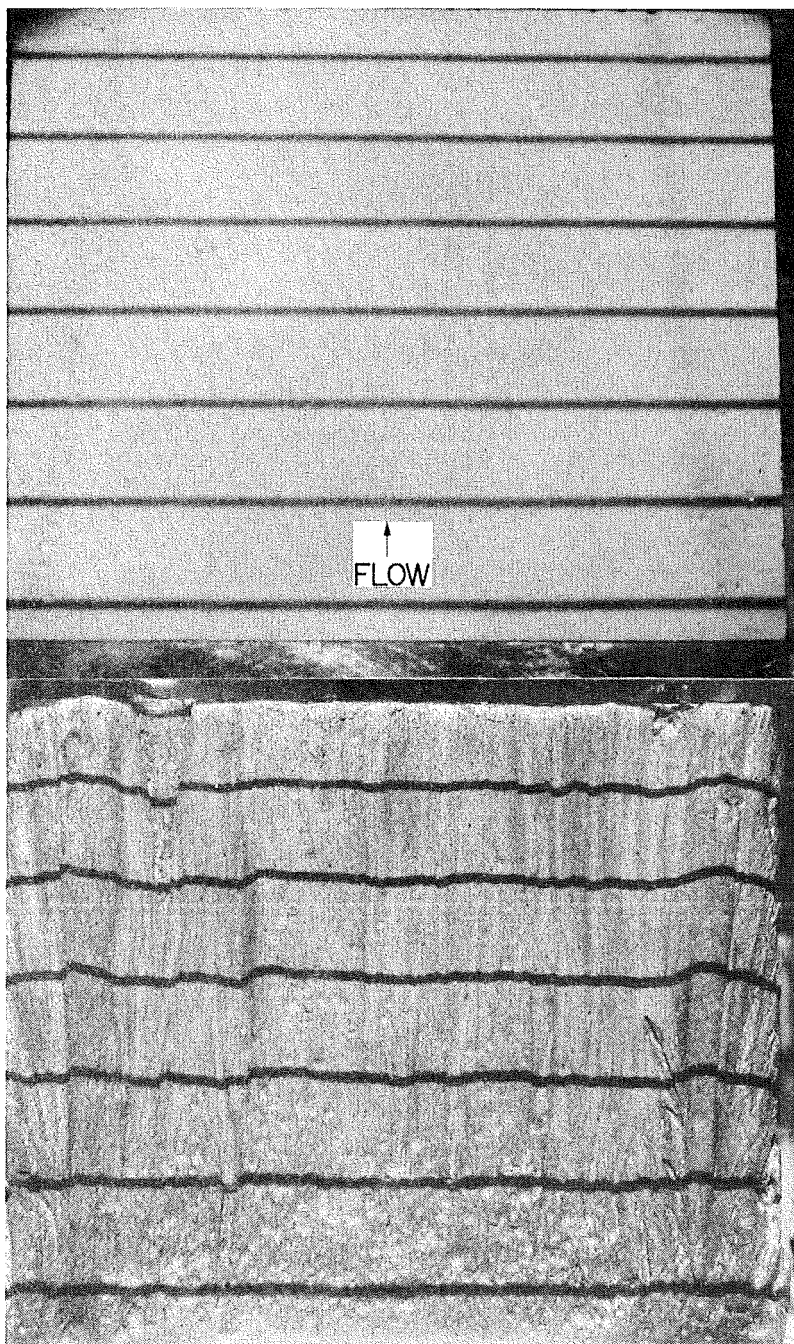
c. $\theta_w = 38$ deg ($\dot{q}_0 \approx 15$ Btu/ft²-sec), sample No. 6, CPR 421
Figure 14. Concluded.

Sample No. 34
CPR 421
Time of Picture,
sec

 ≈ 6

\dot{q}_0 , Btu/ft²-sec

Variable
(See Fig. 8)



≈ 600

Figure 15. Photographs obtained during trajectory C run.

30

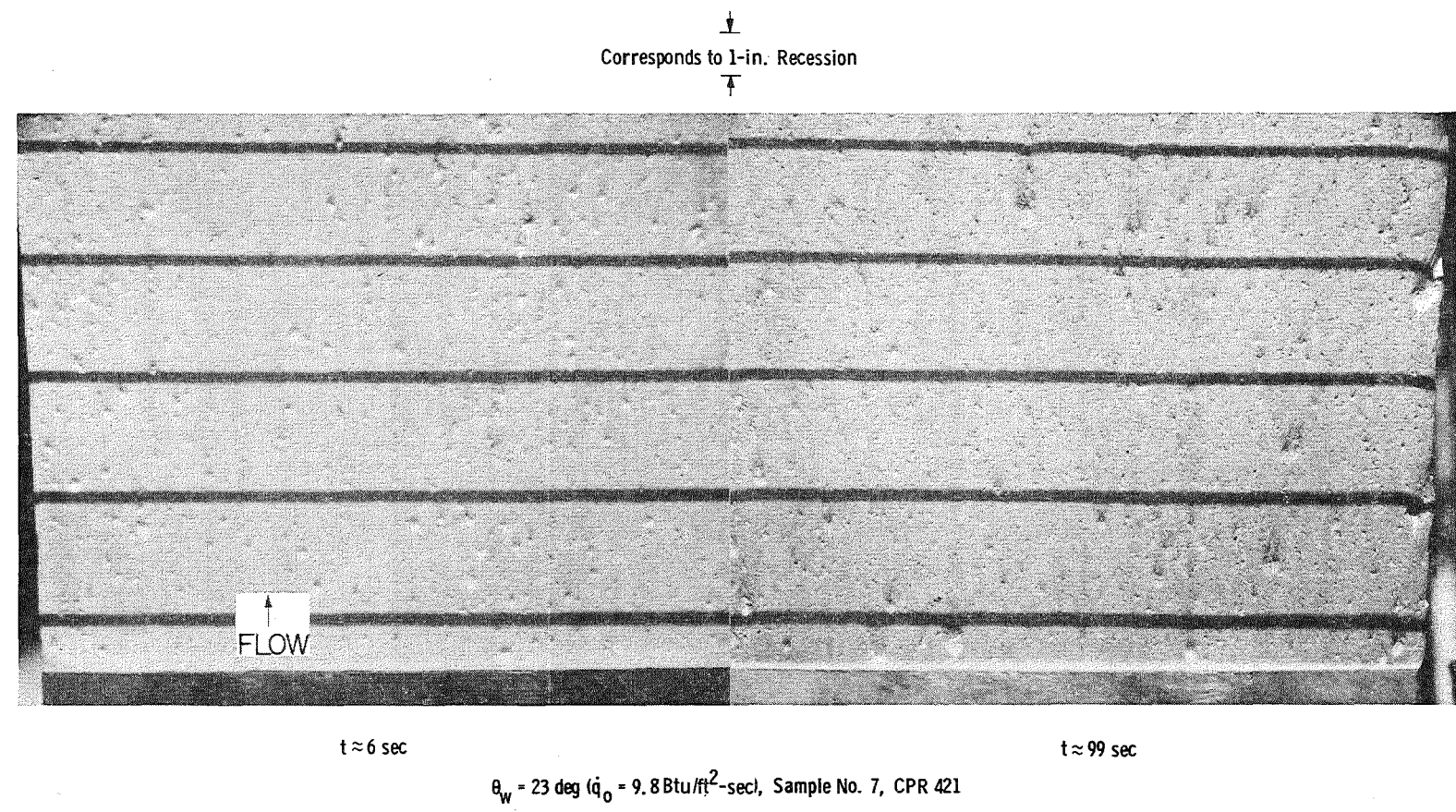
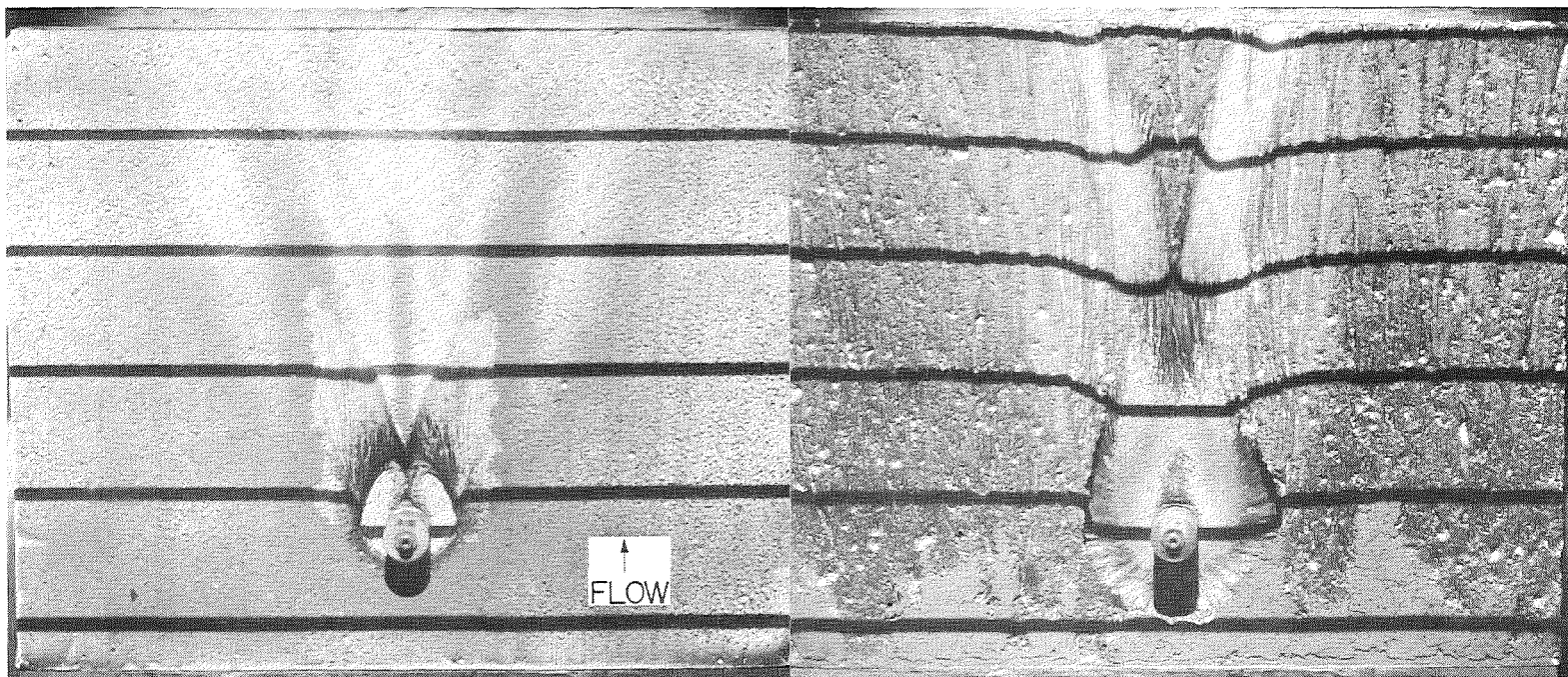


Figure 16. Photographs illustrating the lack of erosion at $T_o = 1080^\circ\text{F}$.



$t \approx 4 \text{ sec}$

$t \approx 20 \text{ sec}$

$\theta_w = 18 \text{ deg}$ ($\dot{q}_0 = 8.0 \text{ Btu/ft}^2\text{-sec}$), Sample No. 51

Figure 17. Photographs illustrating the effect of a protuberance on CPR 421.

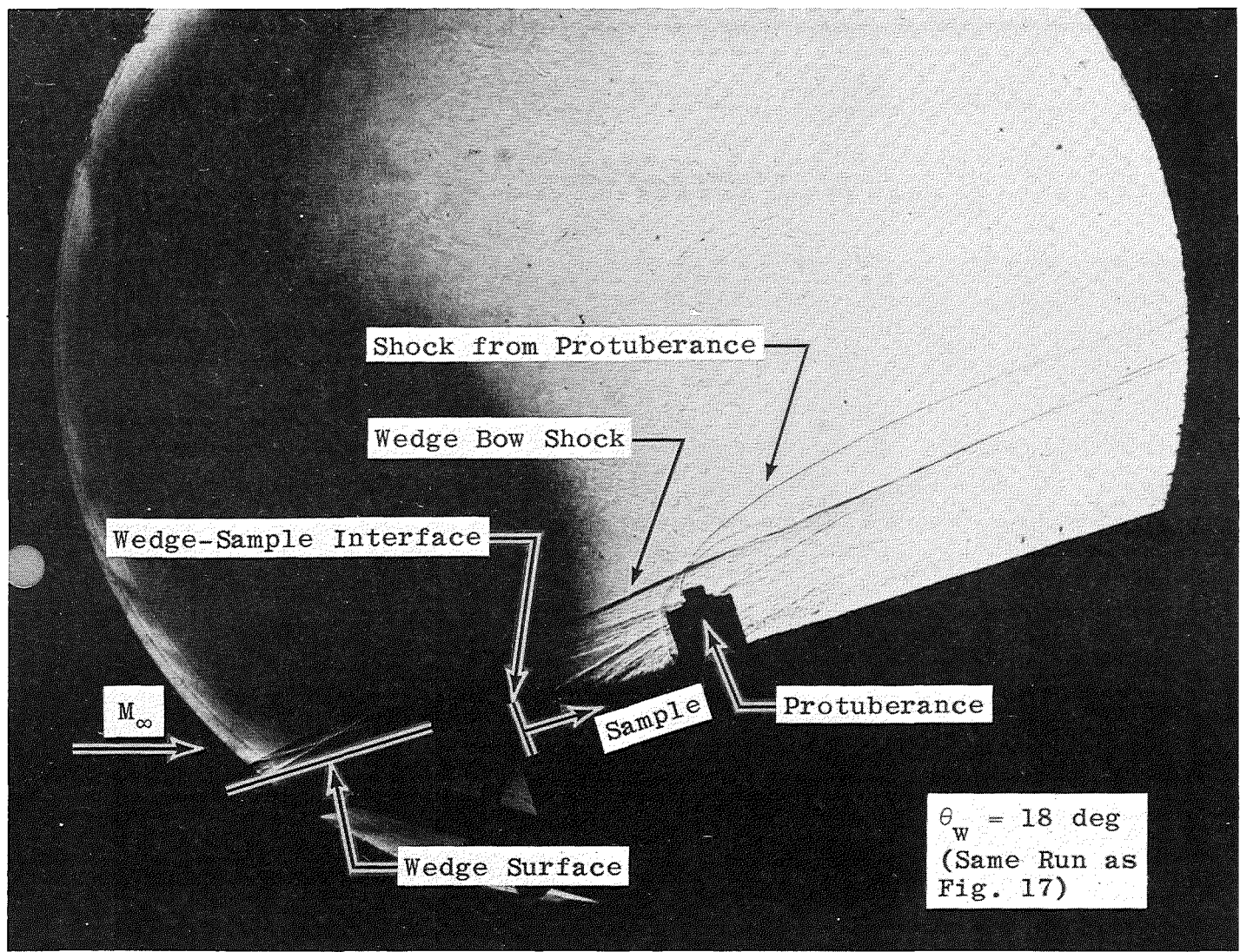


Figure 18. Schlieren photograph of flow field around protuberance.

Table 1. Description of Material Samples

| Sample Numbers | Thickness, in. | Remarks |
|--|-------------------|---|
| 1-8, 10-12, 14, 15, 17, 19-24, 26, 29-37, 43-45, 49 | 1.0 | Machined surface, uncoated CPR 421 |
| 27, 39-42, 44, 50-52 (Protuberance on Sample 51) | 1.0 | Machined surface, coated CPR 421 |
| 57, 58, 67, 69 | 1.75 | Machined surface, uncoated CPR 421 |
| 64, 66 | 1.75 | Machined surface, coated CPR 421 |
| 61-63, 65 | 1.75 | Net spray, uncoated CPR 421 |
| 64, 65 | 1.75 | Net spray, coated CPR 421 |
| 46-48 | 1.0 | Machined surface, coated CPR 421 (with defects) |
| 201, 203 | 0.5 | SLA-561s net spray, coated |
| 202 | 0.5 | SLA-561s net spray, coated, with protuberance |
| 101 | 1.0 | Machined surface, uncoated BX 250 |

Table 2. Test Summary

| M_∞ | P_o , psia | T_o , °F | H_o , Btu/lbm | Re_∞ , in. ⁻¹ | θ_w , deg | Type Data | Sample Numbers |
|------------|-----------------|---------------|--------------------|------------------------------------|---------------------|-------------------|--|
| 10 | 1800 | 1440 | 475 | 0.191×10^{-6} | 0 | [G] | |
| ↓ | ↓ | ↓ | ↓ | ↓ | 6 | [G], [P] | |
| ↓ | ↓ | ↓ | ↓ | ↓ | 9 | [G], Samples | 26, [29] |
| ↓ | ↓ | ↓ | ↓ | ↓ | 12 | [G],[P], Samples | 5, 10, 11, 12 |
| ↓ | ↓ | ↓ | ↓ | ↓ | 15 | [G], [P] | |
| ↓ | ↓ | ↓ | ↓ | ↓ | 18 | [G], [P], Samples | [1], [2], [4], 8, 14, 27, 35, 37, 51, 60, 69, [101], 203 |
| ↓ | ↓ | ↓ | ↓ | ↓ | 20 | [G], [P], Samples | 15, 17, 20 |
| ↓ | ↓ | ↓ | ↓ | ↓ | 23 | [P] | |
| ↓ | ↓ | ↓ | ↓ | ↓ | 23.5 | [G], Samples | 3, 19, 21, [24], 57 |
| ↓ | ↓ | ↓ | ↓ | ↓ | 27.25 | [G] | |
| ↓ | ↓ | ↓ | ↓ | ↓ | 38 | Sample | [6] |
| ↓ | ↓ | ↓ | ↓ | ↓ | A | Sample | 22, 23, 30, 32, 38, 39, 40, 43, 45, 46, 47, 48, 50, 52, 61, 62, 64, 66, 67, 68, 201, 202 |
| ↓ | ↓ | ↓ | ↓ | ↓ | B | Sample | 31, 33, 42, 44, 49, 58, 65, |
| ↓ | ↓ | ↓ | ↓ | ↓ | C | Sample | [34], 41, 63 |
| ↓ | ↓ | 1080 | 375 | 0.280×10^{-6} | 18 | Sample | 36 |
| ↓ | ↓ | 1080 | 375 | 0.280×10^{-6} | 23 | Sample | [7] |

LEGEND: G - Heat-Transfer Gage Data
P - Pressure Data
[X] - Data Presented in This Report

A,B,C - Variable Wedge Angle Runs
(See Fig. 8)

NOMENCLATURE

| | |
|-----------------|--|
| CF | Heat gage calibration factor, (Btu/ft ² -sec)/mv |
| C _p | Specific heat of air, Btu/lbm, °R |
| ΔE | Heat gage electrical output, mv |
| H ₀ | Total enthalpy of free-stream airflow, Btu/lbm |
| K | Heat gage temperature scale factor, °R/mv |
| M _∞ | Free-stream Mach number |
| p | Pressure, psia |
| \dot{q} | Heating rate, Btu/ft ² -sec |
| \dot{q}_0 | Calculated heating rate for T _w = 0 [see Eq. (4)], Btu/ft ² -sec |
| Re _∞ | Free-stream Reynolds number per inch |
| S.F. | Scale factor for grid line projection system, in. ⁻¹ (see Fig. 6) |
| St _∞ | Stanton number [see Eq. (3)] |
| T | Temperature, °R or °F as noted |
| ΔT | Heat gage disk temperature differential, °R |
| t | Time sample exposed to airflow, sec |
| V _∞ | Free-stream air velocity, ft/sec |
| x | Distance along wedge surface and normal to leading edge (see Fig. 3), in. |
| y | Spanwise distance from centerline of wedge (see Fig. 3), in. |
| θ _w | Wedge angle relative to free-stream velocity vector, deg |
| ρ _∞ | Free-stream air density, lb/ft ³ |

SUBSCRIPTS

- G Gage case temperature
- o Measured tunnel stilling chamber conditions (Also note \dot{q}_o defined above)
- w Wall conditions
- ∞ Free-stream conditions